MoS_2 with structure tuned photocatalytic ability for degradation of methylene blue

MoS_2 with structure tuned photocatalytic ability for degradation of methylene blue

Yulan Li *, Fei Xiang, Wenhao Lou, Xinlun Zhang

School of Materials and Energy, University of Electronic Science and Technology of China, Chengdu, China

*Corresponding author e-mail: liyl03@uestc.edu.cn

Abstract. In this work, a series of nanostructured molybdenum disulfide (MoS_2) with various morphologies, such as spherical, flower-like, coil and hollow were synthesized via a one-step hydrothermal method. The photocatalytic properties of as obtained MoS_2 were evaluated by degrading methylene blue (MB) under visible light. Interestingly, the flower-like MoS_2 exhibited the best photocatalytic activities. It is ascribed that the suitable porous structures of flower-like MoS_2 can increase the number of exposed active sites, which facilitate the efficient adsorption and transfer of MB to the active sites. Meanwhile, the special structure of flower-like MoS_2 can improve light absorption efficiency owing to the increasing of light paths. Furthermore, its 2D stacked petals possess abundant active sites, which will effectively affect the photocatalytic efficiency. This study indicates that the surface area of nanomaterials is not a dominated factor in photocatalytic performance. The surface morphology has a great influence on the photocatalytic performance, which provides a feasible guide for synthesizing efficient photocatalytic nanomaterials.

Keywords: hydrothermal method, molybdenum disulfide, photodegradation, nanostructure.

1. Introduction

Since chemical related products entered people's lives in the last century, lots of natural products have been replaced by chemical products. Although the various chemical products facilitates people's lives, they also bring pollution in our environment. For example, in the textile, cosmetics, food, pesticide and plastics industries, a large amount of organic dyes and wastewater containing organic molecules are discharged into rivers and groundwater. Such pollutants are toxic and difficult to be degraded. It is a big challenge to resolve these pollutantsat present. In recent years, visible-light photodegradation technology became a promising approach in the environmental protection field.

Recently, the molybdenum disulfide (MoS_2) nanostructures have attracted considerable attention in various scientific fields for their unique chemical and physical properties.[1,2] The two dimensional (2D) layered MoS_2 has aroused increasingly interests in industrial and scientific fields, and has wide applications in sensors,[3,4,5] photocatalysis,[6,7] dye-sensitized solar cells,[8] batteries and so on.[9,10] In the photocatalysis field for producing hydrogen or degrading organic pollutants in water,[11] 2D MoS_2 nanomaterials were widely concerned by scientists for their narrow band gap (close to 1.2 eV),

which leads a prominent absorption in the visible light area.[12,13] Thus, the MoS_2 nanomaterials have strong utilization of sunlight and potential application in photocatalytic activities.

The noble metal (Ag, Au and Pt) decorated nanomaterials have splendid absorption in the visible light region owing to the surface plasma resonances.[14,15] However, the high cost of noble metal restricts their further large-scale applications.[16,17] The utilization of many other photocatalysts such as Cr[18,19] are also limited since their toxicity, relatively lower production rate and instability. Considering these, the MoS_2 nanomaterials are certainly worth to be investigated in photocatalytic activities for their low cost, earth abundance, excellent stability and high yield. For MoS_2, the morphology could have an important impact on the size of surface area and number of active sites. Thus it is significant to optimize the morphology of MoS_2 nanostructures and achieve the structure-controlled MoS_2 nanomaterials through a facile and environmentally strategy.[20, 21] Among all synthesis strategies, the hydrothermal method is a facile and friendly route to optimize the morphologies of inorganic materials. Here, we successfully synthesized four different morphologies of MoS_2 nanostructures via hydrothermal method, the corresponding morphologies and structures were characterized by SEM, TEM and XRD. The photodegradation performance of as obtained MoS_2 were also evaluated by degrading methylene blue (MB). The flower-like MoS_2 (F- MoS_2) exhibited far better photocatalytic activities than spherical, coil and hollow MoS_2.

2. Experimental

2.1. Synthesis of MoS_2

Different structured MoS_2 was synthesized using Mo-based and S-based precursora by a one-step facile hydrothermal method. [22-24] The preparation procedure of these MoS_2 nanostructures are shown below. The hollow MoS_2 (H-MoS_2): 534 mg of thioacetamide, 230 mg of sodium molybdate and 937mg of oxalic acid were dissolved in 80 mL of deionized (DI) water and magnetically stirred for 30 minutes. The obtained homogeneous solution was transferred into the Teflon autoclave and heated at 200 °C for 22 hours in a drying oven. The F- MoS_2: 1694 mg of sodium molybdate and 1592 mg of L-cystine were dissolved in 80 mL of DI water/ethanol solution (volume ratio is 1:1). After magnetic stirring for 20min, the homogeneous solution was transferred into the Telfon autoclave and heated at 180 °C for 24 hours in a drying oven. The spherical MoS_2 (S-MoS_2): 250 mg of sodium molybdate and 250 mg of L-cystine were dissolved in 80 mL of DI water. After magnetic stirring, the homogeneous solution was transferred into the Telfon autoclave and heated at 200 °C for 12 hours. The coil MoS_2 (C- MoS_2): 483 mg of sodium molybdate, 484.24 mg of L-cystine and 10 uL of CTAB were dissolved in 80 mL of DI water. After magnetic stirring, homogeneous solution was transferred into the Telfon autoclave and heated at 200 °C for 12 hours. After the samples were naturally cool to room temperature, the synthesized products were washed alternately by ethanol and DI water several times. Then the products were dried in vacuum at 60 °C for 8 hours.

2.2. Physicochemical characterization

Powder X-ray diffraction (XRD) measurements were performed on Bruker D8 Advance diffractometer with CuKa1 radiation (λ=0.15406 nm). The morphologies and structures of the samples were carried out by field-emission scanning electron microscopy (FESEM; Hitachi SU-8010) and transmission electron microscopy (TEM; JEOL-2100F). The Brunauer-Emmett-Teller (BET) specific surface area was determined by nitrogen adsorption-desorption isotherm measurements at 77 K (NOVA 2200e).

2.3. Photodegradation measurements

To measure the photodegradation, we measured the light absorption intensity of the MB and MoS_2 mixed solution in different periods under visible light irradiation. The specific experimental method is as follows: First, the light absorption intensity of the standard MB solution was tested as a reference. Then, samples of MoS_2 which have different morphologies were mixed with the prepared standard MB solutions, while a blank control group without MoS_2 was set. After a dark reaction of 30 minutes, the

light absorption intensity of each group was measured, and 1 mL H_2O_2 was added as a stabilizer. The light absorption intensity of each group was then measured every 15 minutes.

3. Results and discussion

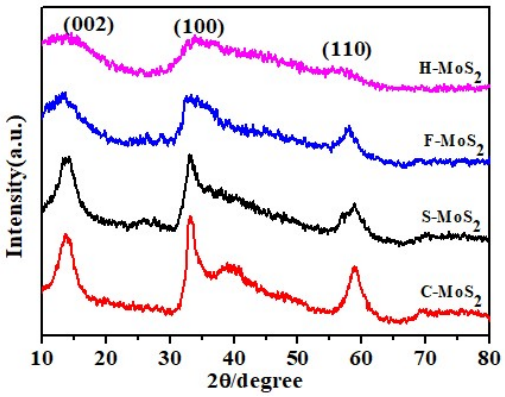

Figure 1. The XRD patterns of MoS_2 samples

The crystal structure and phase purity of MoS_2 samples with different morphologies were characterized by XRD. As shown in Figure1, the XRD spectra patterns of MoS_2 samples with four different morphologies all have obvious characteristic peaks near $2\theta = 14^o$, 32^o and 58^o, in agreement with the (002), (100), and (110) crystal planes, which could be readily indexed to the hexagonal phase of MoS_2 and consistent with the standard powder diffraction file of MoS_2 (JCPDS 37-1492).

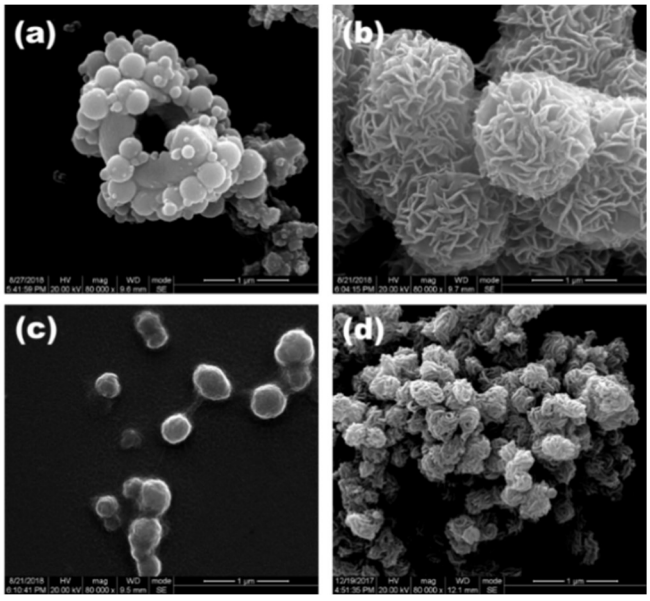

Figure 2. The SEM images of (**a**) H-MoS_2; (b) F-MoS_2; (**c**) S-MoS_2; (d) C-MoS_2.

Figure 2a displays the morphology of H-MoS_2, which clearly shows typical small holes in the microspheres and primary nanoparticles on the surface. The size and number of primary particles were directly affected by the temperature of the hydrothermal reaction. Figure 2b demonstrates the F-MoS_2 with diameter of about 600 nm. The surface of MoS_2 is composed of small-sized 2D-curl layer MoS_2, and the structure is uniform. The thickness of 2D folds are about 30 nm. Figure 2c is S-MoS_2. It is

composed of nanoparticles with diameters about 120 nm, and with less wrinkles and smoother surface. In Figure 2d, the C-MoS_2 with uniform diameter of 280nm is constituted of linear MoS_2.

In order to get further insight on the morphology and structure of MoS_2, the C-MoS_2 was characterized by TEM and high resolution TEM (HRTEM). As shown in Figure 3a and 3b, the C-MoS_2 is composed of linear MoS_2 nanoribbons (the dark area) and nanosheets (the light wrinkle), which are consistent with the SEM images of C-MoS_2 in Figure 2d. HRTEM in Figure 3c shows obvious lattice fringes with a 0.62nm lattice spacing, corresponding to MoS_2 (002) plane. In the selected area electron diffraction pattern (SAED, Figure 3d), it obviously shows that the polycrystalline ring is composed of many dots and two points. This is mainly attributed to the fact that the coil cluster MoS_2 is composed of several single crystal structures with different orientations and belongs to the polycrystalline structure.

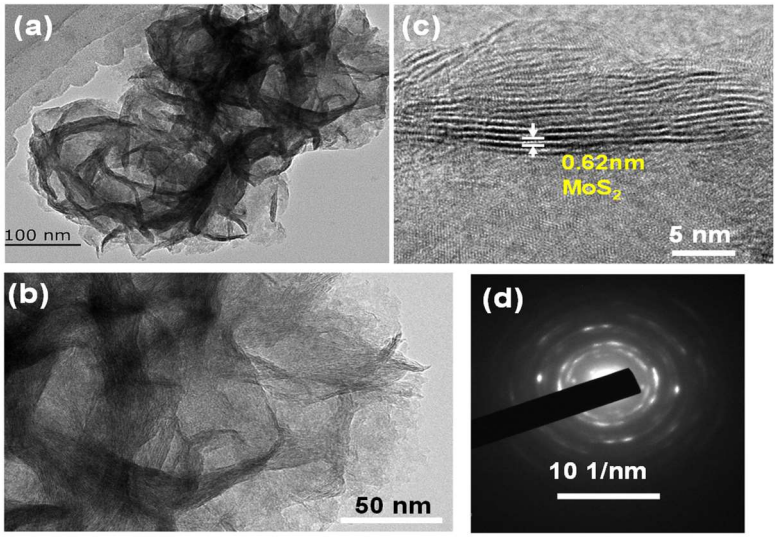

Figure 3. (a and b) TEM images of C-MoS_2; (c) the HR-TEM image of C-MoS_2; (d) the SAED of C-MoS_2

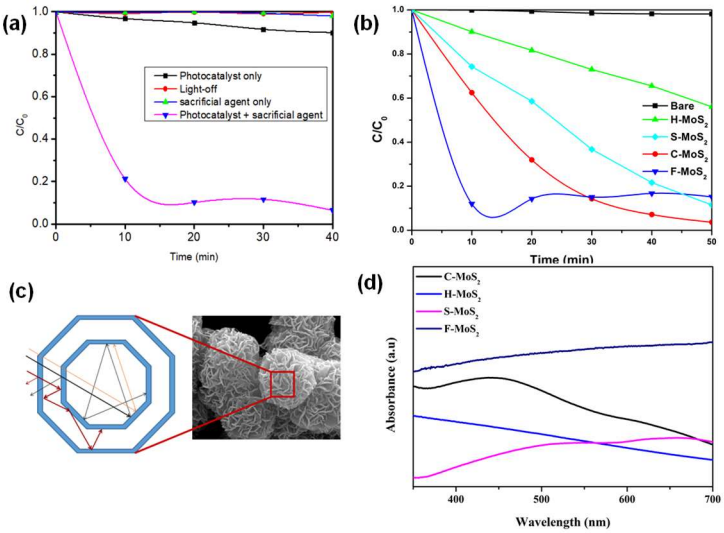

Figure 4. (a) the effect of photocatalyst and sacrificial agent on the degradation MB; (b) the normalized decrease concentration C/C_0 of the MB solution containing different catalysts; (c) the schematic of optical reflection and scattering effects for F-MoS_2 sample; (d) the optical absorption spectra of MoS_2 with different morphologies.

In order to evaluate the photocatalytic performance of as synthesized MoS_2 nanomaterials, the photodegradation of MB was carried out in visible light. It can be visually compared the absorption changes in photocatalytic degradation of MB with or without semiconductor catalysts. Meanwhile the effect of sacrificial agent, hydrogen peroxide (H_2O_2), on photodegradation was also investigated. As shown in Figure 4a, MB is hardly degraded in the absence of catalyst or sacrificial agent. When the semiconductor catalyst and the sacrificial agent H_2O_2 co-exist in the solution, the photodegradation efficient is remarkably improved. This result indicate that the semiconductor catalyst displays a significant photocatalytic activity when combining with the H_2O_2 sacrificial agent.

The maximum absorption peak of MB ranges from 660 to 665 nm. According to the standard curve of MB measured previously, the concentration of MB is proportional to the light absorption intensity when it is below 10 mg/L. This characteristic is conformed to the first-order kinetics. In the MB photocatalytic degradation experiment of MoS_2, 1 mL H_2O_2 was added as sacrificial agent to enhance photocatalytic activity. The MB degradation efficiencies of MoS_2 with different morphologies are shown in Figure 4b. It can be inferred that the degradation rate of F-MoS_2 is the highest and that of H-MoS_2 is the lowest. This result is probably due to their surface morphologies. It will possess more active sites on MoS_2 surface while the material possesses more folds, which leads to a better degradation performance.

Generally, in the process of semiconductor photocatalysis, the specific surface area of photocatalysis is one of the important factors which affects the photocatalytic efficiency[25,26]. In this research, the porous structures of MoS_2 with four different morphologies were measured by BET. The specific surface area and pore size distribution of MoS_2 were shown in Figure 5.. The specific surface area of MoS_2 with four morphologies is: H-MoS_2 (27.82 m^2 g^{-1}), F- MoS_2 (5.28 m^2 g^{-1}), S-MoS_2 (24.48 m^2 g^{-1}) and C-MoS_2 (15.71 m^2 g^{-1}), and the pore size is mainly about 2.8 nm. It can be seen from the SEM image of H-MoS_2 in Figure 2a that, H- MoS_2 displays the largest specific surface area of 27.82 m^2 g^{-1} although the particle size of H-MoS_2 is larg. In comparison with the MB degradation rate of MoS_2 with different morphologies in Figure 4b, an interesting phenomenon was found that the larger the specific surface area, the lower the MB photodegradation rate of MoS_2, suggesting that the specific surface area is not the only factor affecting the photocatalytic activity of semiconductor [25-28]. Because the photocatalytic reaction is driven by light absorption, but the specific surface of the material is not necessarily exposed to the light. For example, the inside of the pores in H-MoS_2 cannot be illuminated, which means it is not the effective specific surface area.

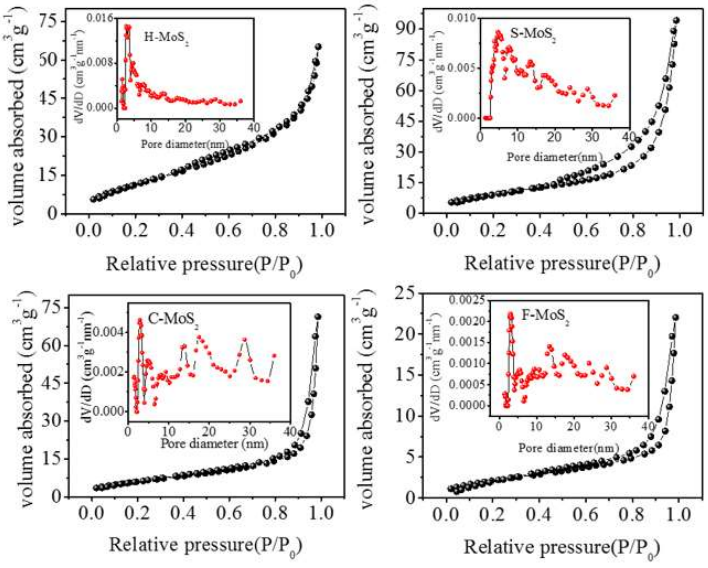

Fig 5. The BET and pore size distribution of MoS_2 with different morphologies: (a) H-MoS_2; (b) S-MoS_2; (c) C-MoS_2; (d) F-MoS_2

For few layer MoS_2, the band gap increases as the number of layers decreases. The bulk MoS_2 has a narrow band gap, which is close to 1.2 eV. Thus, for MoS_2 with different morphologies, the effect of bandgap changes on photocatalysis could be negligible. Due to different surface structures such as mesopores and shapes, MoS_2 with different morphologies have different photocatalytic properties. The influence of morphology on photocatalytic performance is mainly divided into three aspects: 1) enhancing light absorption efficiency. 2) improving molecular dispersion and transmission capacity, increasing the contact between degradants and catalysts. 3) increasing the number of active sites. Specific surface area does not play a decisive role in the performance of photocatalysts.

In the photocatalytic process, only possessing appropriate thermodynamic characteristics (such as appropriate band gap and CV/BV position) can't guarantee excellent photocatalytic effect. The overall photocatalytic performance of semiconductor photocatalysts is affected by many factors, which include micron and nano-scale structures, adsorption capacity, surface/interface morphology, promoter, crystallinity and material composition, etc.[29-35].

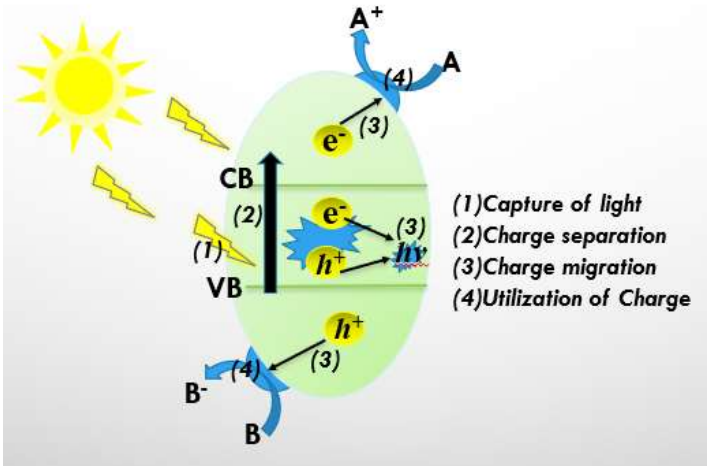

Fig 6. Four phases of photocatalytic process

Generally, the photocatalytic process of semiconductor is divided into four stages as shown in Figure 6. 1) Light capture: a specific wavelength of light irradiated on a semiconductor catalyst is captured. 2) Charge separation: semiconductor catalysts absorb energy, resulting in photogenerated electron-hole pairs. 3) Charge migration: photogenerated electrons and holes migrate in semiconductor catalysts, some migrate to the surface of semiconductor and some recombine in the materials. 4) Utilize the electric charge produces oxidation and reduction reactions on the surface to obtain the desired substances. Therefore, the photocatalytic efficiency is closely related to the efficiency of the four processes of photocatalytic reaction. This is expressed by equation as follows[36,37]:

$$\eta_c = \eta_{abc} \times \eta_{cs} \times \eta_{cmt} \times \eta_{cu} \quad (1)$$

η_c is the conversion efficiency of solar energy, η_{abc} is the absorption efficiency of light, η_{cs} is the excitation/separation efficiency of charge, η_{cmt} is the efficiency of charge transfer and transmission, and η_c is the charge utilization efficiency of photocatalytic reaction.

Figure 4c shows the scheme of reflection and scattering effects of petal folds on light in F-MoS_2. Compared with MoS_2 smooth surface, the flower-like layer structure, which are generated during the formation of photocatalyst, can increase the number of light paths, the interaction time between light and catalyst, and the light absorption efficiency. Figure 4d shows the optical absorption spectra of MoS_2 with different morphologies at the same concentration. The results clearly indicate that optical absorption intensity is relative to the structure of MoS_2. Owing to the light scattering effect, light contact

area and absorption flux increase. At the same mass concentration, the light absorption efficiency of F-MoS_2 is the highest. It can be inferred that the enhancement of light absorption is affected by light scattering effect. Increasing the fold structure of photocatalyst is beneficial to improve light capture ability and overall light utilization efficiency.

The molecular size of MB is 1.43nm×0.6nm×0.4nm [38]. The physical adsorption mechanism of MB in micropore (less than 2 nanometer) is similar to that of pore filling, which is controlled by the strong interaction between MB and micropore walls[39,40]. However, the voids of the structures involved in this study are large, almost all of them are distributed over 2 nano-aperture. MB molecule can be effectively transported to the binding site of the molecule surface through the pore formed by the surface fold, and the degraded small molecule and other products can also freely flow out from the reaction site. The coil and flower-like fold structure effectively increase the contact between MB and the active sites of catalysts, and enhance the photocatalytic efficiency.

In addition, increasing the number of effective photocatalytic active sites is another effective way to improve light absorption efficiency and organic compounds transfer. The 2D folded nanostructures of F-MoS_2 provide abundant active adsorption sites and photocatalytic reaction sites, which are advantages to improve the spacial uniformity of active sites in the prepared photocatalysts. These folded nanostructures can significantly reduce the surface recombination of light-induced electrons and holes and improve the collection, transfer and separation efficiency of charge carriers, which is of vital importance for improving the photocatalytic activity.

4. Conclusion

In this study, MoS_2 catalysts with different morphologies are prepared by a one-step hydrothermal method. The morphology, structure, photodegradation and photocatalytic properties of MoS_2 are investigated. In the process of photocatalytic degradation of MB, it is found that the specific surface area of the catalyst is not the determinant of the photocatalytic degradation rate. H-MoS_2 with the largest specific surface area exhibits the lowest MB degradation rate, while F-MoS_2 with the smallest specific surface area shows the highest degradation rate. Photocatalysts with excellent photocatalytic properties have the following characteristics: First, special structures such as folds and layers are conductive to increase light paths and the interaction time between light and photocatalyst, thus the photocatalytic rate could be enhanced. Second, folding or multi-layer structure with suitable size pore will facilitate the dispersion of organic molecules and promote the adsorption-desorption of MB on the active sites. Lastly, the 2D folded nanostructures would provide abundant active sites for photocatalytic reaction, which improve photocatalytic efficiency significantly. In general, the surface morphology has a great influence on the photocatalytic performance, which provide a significant guide for preparing more efficient photocatalytic nanomaterials.

Acknowledgments

We acknowledge the financial support from the Recruitment Program of Global Young Experts of China and Sichuan one thousand Talents Plan.

References

[1] Zhang Y Y, Liu S, Liu W Q, et al. Two-dimensional MoS2-assisted immediate aggregation of Poly-3-hexylthiophene with high mobility[J]. Physical Chemistry Chemical Physics. 2015, 17(41): 27565-27572.

[2] Kim S Y, Park S, Choi W. Variability of electrical contact properties in multilayer MoS2 thin-film transistors[J]. Applied Physics A, 2014, 117(2): 761-766.

[3] Yue Q, Shao Z, Chang S, et al. Adsorption of gas molecules on monolayer MoS2 and effect of applied electric field[J]. Nanoscale Research Letters, 2013, 8(1): 425.

[4] Zhu, Changfeng, Zeng, Zhiyuan, Li, Hai. Single-Layer MoS2-Based Nanoprobes for Homogeneous Detection of Biomolecules[J]. Journal of the American Chemical Society, 2013, 135(16): 5998.

[5] Li H, Yin Z, He Q, et al. Fabrication of single- and multilayer MoS2 film-based field-effect transistors for sensing NO at room temperature[J]. Small, 2012, 8(1): 63-67.
[6] Wu S, Zeng Z, He Q, et al. Electrochemically reduced single-layer MoS_2nanosheets: characterization, properties, and sensing applications[J]. Small, 2012, 8(14): 2264-2270.
[7] Yin Z , Chen B , Bosman M , et al. Au Nanoparticle-modified MoS2 nanosheet-based photoelectrochemical cells for water splitting[J]. Small, 2014, 10(17): 3537.
[8] Yue G, Wu J, Xiao Y, et al. High performance platinum-free counter electrode of molybdenum sulfide-carbon used in dye-sensitized solar cells[J]. Journal of Materials Chemistry A, 2012, 1(4):1495-1501.
[9] Chen S L, Wang L P, Shao R , et al. Atomic structur and migration dynamics of MoS2/LixMoS2 interface[J]. Nano Energy, 2018, 48 :560-569.
[10] Gao P, Wang L P, Zhang Y Y, et al. Atomic-scale probing the dynamics of sodium transport and intercalation induced phase transformations in MoS2[J]. ACS Nano, 2015, 9 (11): 11296-11301.
[11] KOROTEEV, V. O, BULUSHEVA, et al. Charge transfer in the MoS2/carbon nanotube composite[J]. Journal of Physical Chemistry C, 2011, 115(43): 21199-21204.
[12] Hu K H, Xian G H, Yu F X, et al. The effect of morphology and size on the photocatalytic properties of MoS2[J]. Reaction Kinetics Mechanisms & Catalysis, 2010, 100(1): 153-163.
[13] Wang M, Li G, Xu H, et al. Enhanced lithium storage performances of hierarchical hollow MoS_2nanoparticles assembled from nanosheets.[J]. Acs Applied Materials & Interfaces, 2013, 5(3): 1003-1008.
[14] Wang M, Ye M, Iocozzia J, et al. Plasmonic photocatalysis: Plasmon-mediated solar energy conversion via photocatalysis in noble metal/semiconductor composites[J]. Advanced Science, 2016, 3(6): 1600024.
[15] Li X, Guo S, Kan C, et al. Au multimer@MoS2 hybrid structures for efficient photocatalytical hydrogen production via strongly plasmonic coupling effect[J]. Nano Energy, 2016, 30: 549-558.
[16] Zhang K, Zhao Y, Zhang S, et al. MoS2 nanosheet/Mo2C-embedded N-doped carbon nanotubes: synthesis and electrocatalytic hydrogen evolution performance[J]. Journal of Materials Chemistry A, 2014, 2(44): 18715-18719.
[17] Ma C B, Qi X, Chen B, et al. MoS2 nanoflower-decorated reduced graphene oxide paper for high-performance hydrogen evolution reaction.[J]. Nanoscale, 2014, 6(11): 5624-5629.
[18] Yu J C, Li G, Wang X, et al. An ordered cubic Im3m mesoporous Cr-TiO2 visible light photocatalyst[J]. Chemical Communications, 2006, 25(25): 2717-2719.
[19] Guo J, Ouyang S, Peng L, et al. A new heterojunction Ag3PO4/Cr-SrTiO3 photocatalyst towards efficient elimination of gaseous organic pollutants under visible light irradiation[J]. Applied Catalysis B Environmental, 2013, 134: 286-292.
[20] Ma N, Jena D. Charge ccattering and mobility in atomically thin semiconductors[J]. Physical Review X, 2014, 4(1): 313-322.
[21] Perkins F K, Friedman A L, Cobas E, et al. Chemical vapor sensing with monolayer MoS2[J]. Nano Letters, 2013, 13(2): 668-673.
[22] Zhan Y Q, Fan Y, Pan Y, Han Li, et al. Construction of advanced poly(arylene ether nitrile)/multi-walled carbon nanotubes nanocomposites by controlling the precise interface[J]. Journal of Materials Science, 2016, 51: 2090-2100.
[23] Wan X Y, Zhan Y Q, Zeng G Y, et al. Nitrile functionalized halloysite nanotubes/poly(arylene ether nitrile) nanocomposites: Interface control, characterization, and improved properties[J]. Applied Surface Science, 2017, 30: 1-10.
[24] Zhan Y Q, Wan X Y, Long Z H, et al. Two step hydrothermal synthesis of flowerbud-like magnetite/graphene oxide hybrid with high-performance microwave absorption[J]. Russian Journal of Applied Chemistry, 2016, 89: 297-303.
[25] Hao R, Wang G, Jiang C, et al. In situ hydrothermal synthesis of g-C 3 N 4 /TiO 2 heterojunction

photocatalysts with high specific surface area for Rhodamine B degradation[J]. Applied Surface Science, 2017, 411:400-410.

[26] Zhang L L, Xiong Z, Zhao X S. Pillaring chemically exfoliated graphene oxide with carbon nanotubes for photocatalytic degradation of dyes under visible light irradiation.[J]. Acs Nano, 2010, 4(11):7030-7036.

[27] Wang X C, Yu J C, Ho C M, et al. Photocatalytic activity of a hierarchically macro/mesoporous titania[J]. Langmuir the Acs Journal of Surfaces & Colloids, 2005, 21(6):2552-9.

[28] Yuan Z Y, Ren T Z, Su B L. Hierarchically mesostructured titania materials with an unusual interior macroporous structure[J]. Advanced Materials, 2010, 15(17): 1462-1465.

[29] Zirak M, Moradlou O, Bayati M R, et al. On the growth and photocatalytic activity of the vertically aligned ZnO nanorods grafted by CdS shells[J]. Applied Surface Science, 2013, 273(2): 391-398.

[30] Herney-Ramirez J, Vicente M A, Madeira L M. Heterogeneous photo-Fenton oxidation with pillared clay-based catalysts for wastewater treatment: A review[J]. Applied Catalysis B Environmental, 2010, 98(1):10-26.

[31] Tu W, Yong Z, Zou Z. Versatile graphene-promoting photocatalytic performance of semiconductors: Basic principles, synthesis, solar energy conversion, and environmental applications[J]. Advanced Functional Materials, 2013, 23(40): 4996-5008.

[32] Xu J, Pan C, Takata T, et al. Photocatalytic overall water splitting on the perovskite-type transition metal oxynitride CaTaO2N under visible light irradiation[J]. Chemical Communications, 2015, 51(33): 7191.

[33] Paiano P, Prete P, Lovergine N, et al. Effect of precursors stoichiometry on morphology, crystallinity and electrical properties of ZnTe epilayers grown on (100)GaAs by MOVPE[J]. Crystal Research & Technology, 2010, 40(10-11): 1011-1017.

[34] Gupta P, Bhargava R, Das R, et al. Static and dynamic magnetic properties and effect of surface chemistry on the morphology and crystallinity of DyCrO3 nanoplatelets[J]. Rsc Advances, 2013, 3(48):26427.

[35] Nortier P, Fourre P, Saad A B M, et al. Effects of crystallinity and morphology on the surface properties ofalumina[J]. Applied Catalysis, 1990, 61(1):141-160.

[36] Li X, Yu J, Low J, et al. Engineering heterogeneous semiconductors for solar water splitting[J]. Journal of Materials Chemistry A, 2015, 3(6):2485-2534.

[37] Tachibana Y , Vayssieres L , Durrant J R . Artificial photosynthesis for solar water-splitting[J]. Nature Photonics, 2012, 6(8):511-518.

[38] Li X, Yu J, Jaroniec M. Hierarchical photocatalysts[J]. Chemical Society Reviews, 2016, 45(9):2603-2636.

[39] Pelekani C, Snoeyink V L. Competitive adsorption between atrazine and methylene blue on activated carbon: the importance of pore size distribution[J]. Carbon, 2000, 38(10): 1423-1436.

[40] Zhan Y Q, Long Z H, Wan X Y, et al. Exfoliated graphite nanoplatelets/poly(arylene ether nitrile) nanocomposites; In situ synthesis, characterization, and enhanced properties[J]. High Performance Polymers, 2016, 29: 1121-1129